Electrostatic free energy for a confined nanoscale object in a fluid

Krishnan, Madhavi

Abstract: We present numerical calculations of electrostatic free energies, based on the nonlinear Poisson-Boltzmann (PB) equation, for the case of an isolated spherical nano-object in an aqueous suspension, interacting with charged bounding walls. We focus on systems with a low concentration of monovalent ions (10−4 M), where the range of electrostatic interactions is long (30 nm) and comparable to the system and object dimensions (100 nm). Locally tailoring the geometry of the boundaries creates a modulation in the object-wall interaction, which for appropriately chosen system dimensions can be strong enough to result in stable spatial trapping of a nanoscale entity. A detailed view of the underlying mechanism of the trap shows that the physics depends predominantly on counterion entropy and the depth of the potential well is effectively independent of the object's dielectric function; we further note an appreciable trap depth even for an uncharged object in the fluid. These calculations not only provide a quantitative framework for understanding geometry-driven electrostatic effects at the nanoscale, but will also aid in identifying contributions from phenomena beyond mean field PB electrostatics, e.g., Casimir and other fluctuation-driven forces.

DOI: https://doi.org/10.1063/1.4795087

Electrostatic free energy for a confined nanoscale object in a fluid

Madhavi Krishnan

Citation: The Journal of Chemical Physics **138**, 114906 (2013); doi: 10.1063/1.4795087
View online: http://dx.doi.org/10.1063/1.4795087
View Table of Contents: http://scitation.aip.org/content/aip/journal/jcp/138/11?ver=pdfcov
Published by the AIP Publishing

Electrostatic free energy for a confined nanoscale object in a fluid

Madhavi Krishnan[a)]
Institute of Physical Chemistry, University of Zurich, Winterthurerstrasse 190, 8057 Zurich, Switzerland and Institute of Physics, University of Zurich, Winterthurerstrasse 190, 8057 Zurich, Switzerland

(Received 11 December 2012; accepted 26 February 2013; published online 21 March 2013)

We present numerical calculations of electrostatic free energies, based on the nonlinear Poisson-Boltzmann (PB) equation, for the case of an isolated spherical nano-object in an aqueous suspension, interacting with charged bounding walls. We focus on systems with a low concentration of monovalent ions ($\lesssim 10^{-4}$ M), where the range of electrostatic interactions is long ($\sim$30 nm) and comparable to the system and object dimensions ($\sim$100 nm). Locally tailoring the geometry of the boundaries creates a modulation in the object-wall interaction, which for appropriately chosen system dimensions can be strong enough to result in stable spatial trapping of a nanoscale entity. A detailed view of the underlying mechanism of the trap shows that the physics depends predominantly on counterion entropy and the depth of the potential well is effectively independent of the object's dielectric function; we further note an appreciable trap depth even for an uncharged object in the fluid. These calculations not only provide a quantitative framework for understanding geometry-driven electrostatic effects at the nanoscale, but will also aid in identifying contributions from phenomena beyond mean field PB electrostatics, e.g., Casimir and other fluctuation-driven forces. © *2013 American Institute of Physics*. [http://dx.doi.org/10.1063/1.4795087]

I. INTRODUCTION

Recent advances in nanofabrication technology have fostered novel developments in confined soft matter research.[1–8] Experiments show that when confined at submicrometer length scales, the dynamics and transport properties of colloidal particles, globular macromolecules, and polyelectrolytes respond dramatically to the geometry of boundaries.[1,3,7,8] Perturbations in bounding surfaces introduce a spatial modulation of the object-wall interaction giving rise to free energy landscapes that not only spatially trap objects, but in conjunction with an external driving force, can be engineered to sort and sieve matter. For example, in confined systems, the periodic modulation of electrostatic interactions and configurational entropy of semi-flexible objects have been exploited to demonstrate sieving.[4] The electromagnetic variant of this principle utilizes optical lattices or an array of optical traps, where objects in free solution transported through the lattice are sorted based on their relative polarizability.[9,10] Further examples of this principle involve the manipulation of micrometer-scale entities such as droplets, colloids, and DNA by geometric modulation of the interfacial free energy,[11] gravitational potential energy,[12] the critical-Casimir force in binary fluid mixtures,[13] and the electrostatic interaction with corrugated lipid membranes,[14] to name a few. Although the theme of transport through modulated potential energy landscapes pervades solid-state physics and arises in many natural processes, controlled experimental realizations of similar concepts in nanoscale soft matter systems has had relatively recent beginnings but holds great promise.

Electrostatics at the nanoscale is a multifaceted and growing field with much to offer in terms of experiment, technology, and theory.[15] Rigorous calculations of geometry-dependent effects have proved vital in disparate areas, e.g., colloidal self-assembly where the shape of the particle itself, rather than spatial modulation of the environment, profoundly influences interparticle interactions.[16] At the level of the fluid-solid interface, electrofluidic gating, fluidic diodes, and transistors have been realized through the spatial manipulation of charge densities in nanofluidic devices.[17,18] More recently, we established the use of geometric modulation of the electrostatic interaction between an object in a fluid and its neighbouring surfaces to stably trap and orient it.[7,8]

Here, we discuss in detail the electrostatic interaction for a nanoscale entity suspended in a fluid, thermally sampling the gap between parallel topographically structured charged walls, and present the theoretical underpinnings of the recently demonstrated electrostatic fluidic trap.[7] The system consists of a submicrometer diameter spherical particle bounded by two parallel glass or SiO_2 walls. In contact with water, ionizable chemical groups at the surfaces dissociate resulting in surfaces that carry a net negative charge. Close to an isolated ionized surface, the electrostatic potential, ψ may be taken to decay exponentially with distance as $\psi(z) = \psi_0 \exp(-\kappa z)$, where ψ_0 represents the surface value and κ^{-1} denotes the "Debye length," which for a monovalent electrolyte is given by $\sqrt{\frac{2c_0e^2}{\varepsilon\varepsilon_0 k_B T}}$. Here, c_0 represents the salt concentration in the electrolyte at infinity, $\varepsilon\varepsilon_0$ is the permittivity of the medium, and e is the elementary charge. In a slit created by two charged planes in contact with a fluid and separated by a gap $2h$, the electrostatic potential decays monotonically from the walls and gives rise to a minimum midway between them. For low values

a)Author to whom correspondence should be addressed. Electronic mail: madhavi.krishnan@uzh.ch.

of ψ_0, this midplane potential can be taken to be simply additive and is given by $\psi_m = 2\psi_0 \exp(-\kappa h)$. A local increase in width of the gap by d perturbs the local potential minimum which is now $\psi_m = 2\psi_0 \exp[-\kappa(h + d/2)]$. So a point charge q, traversing a width modulation in the gap would experience a change in electrostatic energy given by $\Delta U = 2q\psi_0 \exp(-\kappa h)[1 - \exp(-\kappa d/2)]$. When $d \to 0$, i.e., the width modulation vanishes, the slit consists of two flat parallel walls facing each other, and $\Delta U \to 0$. For large κd on the other hand, $\Delta U = 2q\psi_0 \exp(-\kappa h)$ which implies a local potential well in which a charged object can be spatially trapped for an average time that scales as $\exp(\Delta U/k_B T)$ (Ref. 19). These simple arguments are based on the linearization of the governing equations (Eq. (1)), which is valid for low surface potentials or far away from surfaces. While this picture does furnish physical insight into how geometrical modulation of a gap can spatially trap a point object, it is not quantitatively correct since it only considers the electrostatic self-energy of the object, and ignores not only the extended nature of the experimental entity but more importantly, the electrostatic energy and entropy of the rest of the system, particularly those of the counterions in the fluid.

II. CALCULATING POISSON-BOLTZMANN (PB) FREE ENERGIES

We present calculations of electrostatic system free energies for this system based on mean field Poisson-Boltzmann theory[20–22] and analyze in detail the various energetic and entropic contributions as a function of particle position in the geometrically modulated slit. The first step in a free energy calculation for a system of charged entities involves obtaining the spatial electrostatic potential distribution by solving the nonlinear PB equation subject to appropriate boundary conditions.[23,24] Given the spatial distribution of the electrostatic potential, $\phi(x, y, z)$, all quantities that constitute the free energy can be directly obtained by integration, as shown in Eqs. (2)–(5). The equilibrium state of a macroscopic system corresponds to one of minimum free energy, i.e., Helmholtz free energy for an incompressible system. In order to calculate $\phi(x, y, z)$, we consider a system consisting of a rectangular nanoslit composed of two parallel charged plates with the gap in between filled by an electrolyte of a given ionic strength and in contact at the extremities with an infinite reservoir of the same electrolyte. The system is open in the sense that it is free to exchange ions with the electrolyte bath outside, as is generally true in experiments. This problem has been studied previously for the confined fluidic systems as well as in the context of charged lamellar membranes, which for the purpose of electrostatics is a good physical analog of the charged nanoslit.[22–24] In our calculation, we further modify the geometry of the bounding slit walls to reflect the geometric perturbation introduced in the experiment. We consider a parallel plate geometry with a gap of $2h = 215$ nm where the top surface carries a disc-shaped indentation or "pocket" 200 nm in diameter and 100 nm in depth, as shown in Fig. 1. We also include a spherical nano-object with variable bulk dielectric constant and surface charge in the gap. The diameter of the particle is 80 nm and the solution ionic strength

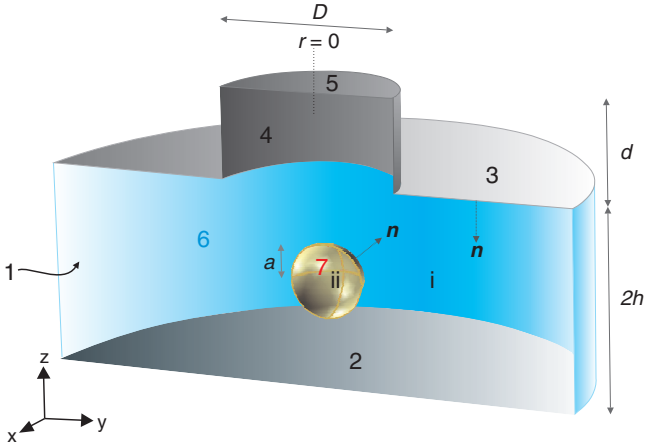

FIG. 1. Sketch of the system geometry considered for the calculation of Poisson-Boltzmann free energies. Domains (i) and (ii) denote the electrolyte-filled, indented slit region and the charge-free particle interior, respectively, while numbered surfaces denote domain boundaries. Values of the geometric parameters used in all calculations are: slit depth, $2h = 215$ nm; pocket depth, $d = 100$ nm and diameter, $D = 200$ nm; particle radius, $a = 40$ nm (shown here) – 100 nm.

0.03 mM unless otherwise noted. This set of parameters was chosen to correspond to those of a recent experimental study where we demonstrated a direct measurement of charge on single particles by electrostatic trapping in harmonic confining potentials.[25]

We write a dimensionless PB equation, for the electrostatic potential $\psi = \frac{e\varphi}{k_B T}$

$$\nabla^2 \psi = (\kappa h)^2 \sinh(\psi), \tag{1}$$

where h represents the half width of the gap and κ represents the inverse Debye length based on the concentration of ions in the electroneutral reservoir.[24] For the interior of the particle, we assume a uniform dielectric environment with dielectric constant given by ε_p and zero space charge density, i.e., $\nabla^2 \psi = 0$. The equations were numerically solved using COMSOL Multiphysics for one half-space of the geometry, as depicted in Fig. 1, applying either constant electric field, $\boldsymbol{n}.\nabla\psi = -\frac{h}{\varepsilon_w \varepsilon_0 k_B T}\sigma_{p,w}$, or constant potential, $\psi_s = \psi_{p,w}$ boundary conditions to all physical surfaces (Table I). Here, $\boldsymbol{n}$ denotes the unit normal directed into the electrolyte region (Fig. 1), $\sigma_{p,w}$, stands for the surface charge density, with subscripts p and w denoting quantities on the particle and wall, respectively, and $\varepsilon_w = 80$ is the dielectric constant of water. The continuity condition $\boldsymbol{n}.\nabla\psi = 0$ is applied on the vertical boundary of the cylindrical electrolyte region far away from the trap (Fig. 1 and Table I). The center of mass of the particle was scanned in space and the spatial distribution of electrostatic potential determined for each new particle location. Electroneutrality of the charge distributions can be verified by integrating over the positive and negative ions in the volume and on the surfaces, so that $n_+ = \int_V c_0 \exp(-\psi) dV$ and $n_- = \int_V c_0 \exp(\psi) dV + \int_A s dA$, where s denotes a dimensionless number density of surface charge. The typical deviation between n_+ and n_- is less than 0.004% which confirms that the obtained potential distributions are indeed physical. In order to derive free energies from these potential distributions,

TABLE I. Equations and boundary conditions for numerical calculations of electrostatic potential in the geometry shown in Fig. 1.

Domain	i – electrolyte ii – particle	Poisson-Boltzmann, $\nabla^2\psi = (\kappa h)^2\sinh(\psi)$ Laplace, $\nabla^2\psi = 0$
Surface	1	Symmetry, $\boldsymbol{n}.\nabla\psi = 0$
	2–5	Surface charge, $\boldsymbol{n}.\nabla\psi = -\frac{h}{\varepsilon_w\varepsilon_0 k_B T}\sigma_w$ or Surface potential, $\psi_s = \psi_w$
	6	Continuity, $\boldsymbol{n}\cdot\nabla\psi = 0$
	7	Surface charge, $\boldsymbol{n}\cdot(\varepsilon_p\nabla\psi\|_p - \varepsilon_w\nabla\psi\|_w) = \frac{h}{\varepsilon_0 k_B T}\sigma_p$ or Surface potential, $\psi_s = \psi_p$

we draw on the theoretical framework established in previous work.[20–22]

The electrostatic free energy of a charge distribution may be analyzed in terms of its electrostatic potential energy and the configurational entropy of the ions and solvent in the electrolyte. The electrostatic potential energy is the same as the field energy or self-energy of a distribution of charges and in its standard dimensional form is given by

$$U_{el} = \frac{\varepsilon\varepsilon_0}{2}\int_V (\boldsymbol{E}\cdot\boldsymbol{E})dV = \frac{1}{2}\int_A \sigma\varphi_s dA + \frac{1}{2}\int_V \rho\varphi dV, \tag{2}$$

where φ_s is the potential at the surface and $\rho = \rho^+ + \rho^- = c_0 e\{\exp(-\psi) - \exp(\psi)\}$ represents the local net charge density in solution. The entropy of mixing of a dilute solution of charges is given by[20,21]

$$\Delta S = k_B\int_V \left\{\sum_i c_0[z_i\psi\exp(-z_i\psi) + \exp(-z_i\psi) - 1]\right\}dV, \tag{3}$$

where subscript i denotes the species of ion (counterion or coion) and $z_i = \pm 1$ denotes its charge. The system free energy is obtained by putting the energy and entropy terms together in $F_{el,c} = U_{el} - T\Delta S$, so that for surfaces that interact at constant charge, we have

$$F_{el,c} = \int_V \left\{\frac{\varepsilon\varepsilon_0}{2}(\boldsymbol{E}\cdot\boldsymbol{E}) - 2c_0 k_B T(\psi\sinh\psi + \cosh\psi - 1)\right\}dV. \tag{4}$$

When considering surfaces interacting at constant potential, we include an additional chemical free energy term, $F_{chem} = -\int_A \sigma\varphi_s dA$ that accounts for the change in free energy due to adsorption of ions at the charged interface.[20] Applying Eq. (2) and recognizing that $\rho\varphi = 2c_0 k_B T\psi\sinh\psi$, the free energy for the constant potential case reads

$$F_{el,p} = \int_V \left\{-\frac{\varepsilon\varepsilon_0}{2}(\boldsymbol{E}\cdot\boldsymbol{E}) - 2c_0 k_B T(\cosh\psi - 1)\right\}dV. \tag{5}$$

The procedure was checked against the calculation for spheres of constant potential and reveals good quantitative agreement with Ref. 20.

Figure 2 presents the various contributions to the total free energy as a function of distance from the trap center. First, we consider the case where the particle and walls interact under the constant and uniform surface charge assumption with charge densities $\sigma_p = -3\times10^{-3}$ e/nm^2 and $\sigma_w = -10^{-2}$ e/nm^2, respectively, estimates that are obtained from particle zeta potential and electroosmotic flow measurements, respectively. We find that the electrostatic self-energy of the system changes little as the object traverses the indentation while the entropy of mixing term changes dramatically (Fig. 2(a)). The entropy of mixing itself contains contributions from the ions (predominantly counterions) and water. As the object traverses the trap, the configurational entropy of the counterions decreases dramatically. Counterion density distributions for center and off-center positions of the particle in the trap in Fig. 2(c) provide qualitative evidence of higher spatial compression of counterions as the particle moves out of the trap and closer to the parallel plate region of the slit. In summary, we find that the dominant contribution to the trap depth comes from the configurational entropy of the counterions, and that the self-energy contribution, although positive, is minimal.

Next, we analyze the system using surfaces of constant and spatially uniform potential rather charge density. The surface of the sphere and the walls were held constant at a potential given by the surface-averaged values obtained from the constant charge density solution with the sphere located at the axial minimum at $r = 0$, and free energies were calculated for each location of the particle using Eq. (5). In this case, we have $\psi_p = -34.5$ mV and $\psi_w = -83$ mV which correspond to surface charge densities $\sigma_p = -3\times10^{-3}$ e/nm^2 and $\sigma_w = -10^{-2}$ e/nm^2, respectively. The spatial free energy profile reveals similar qualitative trends but a quantitative difference compared to the constant charge case, namely, that the predicted well depth at $r = 75$ nm from the trap center is smaller by about 20% (Fig. 2(b)). Here again, we note two contributions to the free energy – a term dependent on the electrostatic self-energy and an entropic term – which display opposing trends: the energetic term attains a maximum while the entropic term goes through a minimum when the particle is at the bottom of the trap ($r = 0$).

It is instructive to view the system as two independent half-spaces about the midplane of the slit, with each functioning like a pair of interacting flat plates. Locations of the sphere in the trap and outside could be taken to correspond to physically to large and small inter-plate separations, respectively, in the upper half-space (Fig. 5(b)). From the perspective of (counter)ion density, this analogy would imply a repulsion when the particle is outside the trap (plates are closer together) compared to when the particle is in it (plates are farther apart), which is indeed captured in the calculation. The

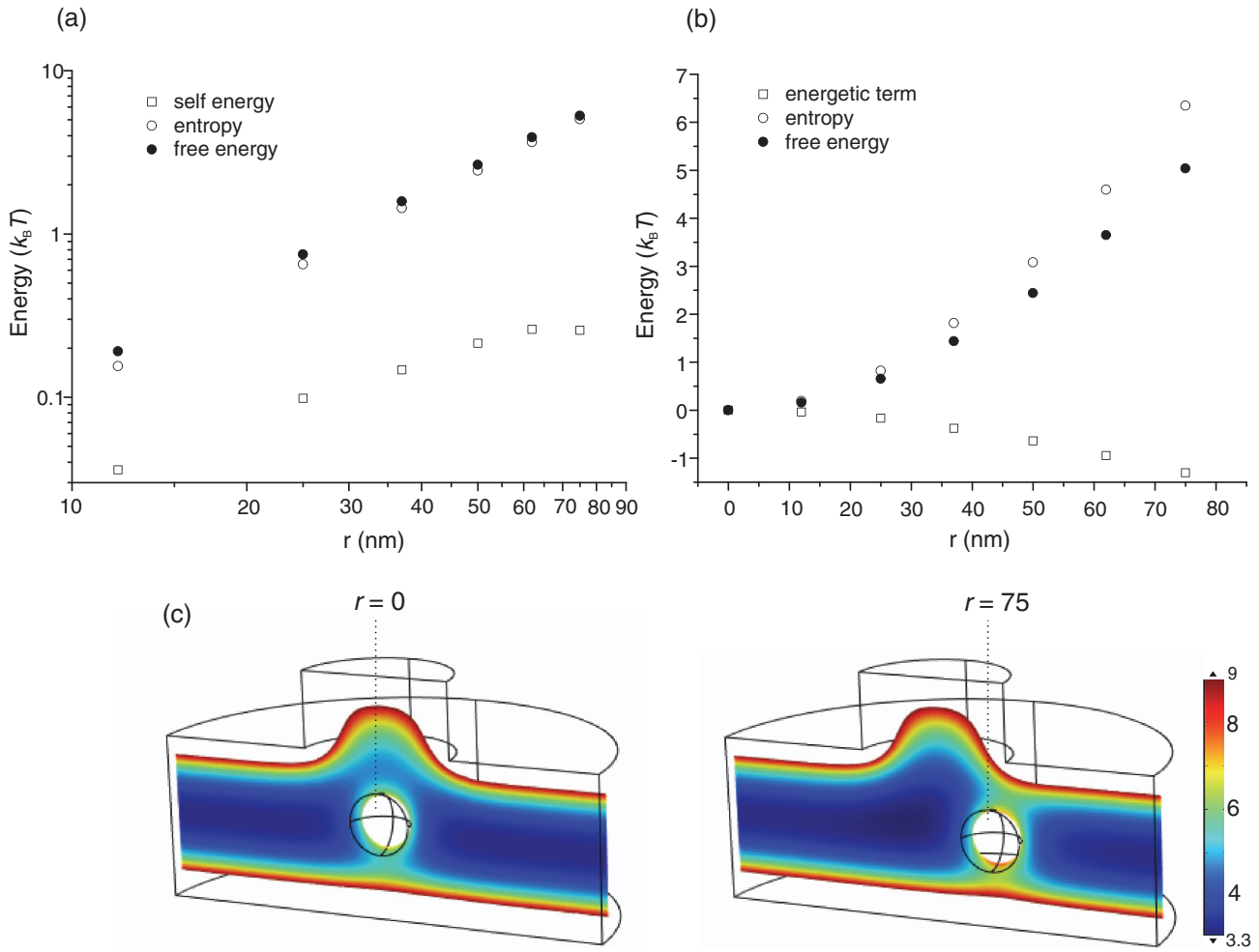

FIG. 2. Radial free energy calculations for a particle of radius $a = 40$ nm, dielectric constant $\varepsilon_p = 0$, in an electrolyte of concentration $c_0 = 0.03$ mM. Radial profiles of electrostatic self-energy, entropy of mixing, and total free energy calculated using boundaries with constant and uniform (a) surface charge density, $\sigma_p = -3 \times 10^{-3}$ e/nm^2 and $\sigma_w = -10^{-2}$ e/nm^2 and (b) electrostatic potential, $\psi_p = -34.5$ mV and $\psi_w = -83$ mV. (c) Cross section of the spatial counterion density in the yz plane for the calculation in (a) presenting the particle at the bottom of the well at $r = 0$ (left) and offset from the bottom, at the axial minimum at $r = 75$ nm (right). Scale bar is in units of c_0.

self-energy of the system, $\frac{\varepsilon\varepsilon_0}{2}\int_V (\boldsymbol{E}\cdot\boldsymbol{E})dV$, whose variation is much smaller, however, behaves differently from the parallel plate scenario for both constant charge and constant potentials cases. We find that when the particle is outside the well there is greater overall curvature in the potential, which gives a higher self-energy, implying a repulsion. This is in contrast to the case of two flat plates – either at constant potential or constant charge – where the reduction in curvature of the potential as the plates approach gives a continuously decreasing self-energy. Nonetheless, the self-energy contribution is small and we find that both the constant charge and constant potential routes yield trapping free energies that are in reasonable agreement. More importantly, similar to the parallel plate case, both share the same fundamental driving mechanism governed by the entropy of the counterions.

In general, the boundary conditions applied in solving the PB equation can dramatically affect both the qualitative and quantitative behavior of a system. The profound influence of boundary conditions is most apparent in the case of dissimilar like-charged surfaces, carrying the same sign of charge, but of different magnitudes. Two such dissimilar surfaces interacting at constant potential can attract at close range, whereas the interaction with constant surface charge predicts only repulsions.[26] Although surfaces with constant charge density present a theoretical idealization, the assumption suffices to explain at least semi-quantitatively the behavior in many experimental situations. Indeed, various kinds of boundary conditions including constant charge, constant potential, mixed charge-potential, and charge regulating boundary conditions have been studied in the literature. Charge regulating boundary conditions present an intermediate case between those of constant charge and constant potential, and account for chemical equilibrium reactions that ultimately determine the charge of an object. These surface chemical equilibria are strongly affected by the local concentration of potential determining ions at the surface (protons for SiOH surfaces) and their incorporation into the model enables the study of more realistic scenarios where net charge of a surface responds to changes in the local electric potential induced either externally, or by the proximity of another charged body.[18,27] For a trapped particle, the interacting surfaces are far from each other (intersurface separation more than 2 effective Debye lengths) and we

argue that the perturbative motion of the particle thermally sampling the region of the free energy minimum does not alter the particle-surface separation enough to warrant the use of a charge regulation condition. We therefore generally use a constant and uniform surface charge condition on all surfaces.

A. Comparing theory with experiment

Figure 3 presents a comparison of calculated free energies with the experimental measurements of the spatial potential, $U(r)$ for single trapped particles. Experimental data for $U(r)$ are taken from Ref. 7, and were obtained by optically imaging the Brownian motion of a trapped particle and converting its normalized radial probability density distribution, $P(r)$ to a local potential via the Boltzmann relation $U(r) = -\ln(P(r))/(P(0))$. Free energy calculations for this system were performed using constant surface charge density for a particle of radius $a = 50$ nm in a slit of depth $2h = 200$ nm, trapped by pockets of diameter $D = 200$ and 500 nm in solutions of ionic strength $c_0 = 0.07$ and 0.17 mM. The calculations correctly capture the broad features observed in the experiment, namely, spatial stiffening of the trap with a reduction in pocket diameter, and a decrease in well depth accompanied by broadening of the potential well in response to an increase in solution ionic strength. We point out that for 100 nm diameter particles trapped by $D = 500$ nm pockets, the experimental data display shallow minima at radial locations offset from $r = 0$. These minima are however not present

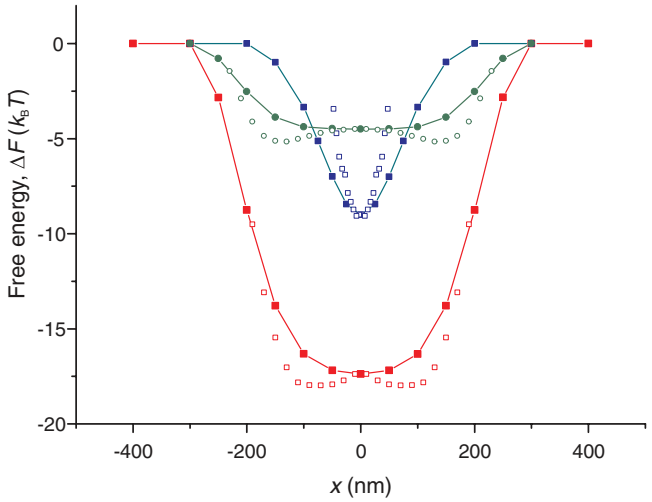

FIG. 3. Comparing experimental measurements (open symbols) with free energy calculations (closed symbols) for different ionic strengths, c_0 and pocket diameters, D. The experimental data shown here are the same as those presented in Ref. 7 for particles of radius $a = 50$ nm confined in a slit of depth $2h = 200$ nm. Data presented are averages over ca. 10 different particles in each of the following cases: $D = 500$ nm, $c_0 = 0.07$ mM (red squares); $D = 500$ nm, $c_0 = 0.17$ mM (green circles) and $D = 200$ nm, $c_0 = 0.07$ mM (blue squares). Charge densities for the particle and walls used in the calculation, $\sigma_p = -3.75 \times 10^{-3}$ e/nm^2 and $\sigma_w = -10^{-2}$ e/nm^2 were estimated from zeta potential and electroosmotic flow measurements respectively. The experimental data are overlaid on the calculation by aligning the values at $x = 0$. In order to facilitate a comparison of the three cases, calculated $\Delta F(x)$ values are referenced against the system free energy far away from the pocket. Solid lines through the closed symbols are provided as a visual guide.

in measurements on 80 nm diameter particles,[25] and are not captured in the free energy calculations which always predict a trapping potential that monotonically increases from the trap center.

Our calculations further demonstrate that for harmonic confining potentials created by $D = 200$ nm pockets, the predicted trap stiffness is a strong function of particle charge.[25] Since existing experimental techniques to determine the charge of particles in solution rely on measurement of the zeta potential which at best serves as an approximate indicator, and in general presents a highly averaged measurement over the sample, quantitative agreement with theory in our case would require that charge density of the particle, σ_p be treated as a fit parameter in the calculation. We recently demonstrated the use of these free energy calculations in conjunction with accurate experimental measurements of the trapping potential to directly determine the charge on single particles.[25]

B. Dielectric function of the object

We now examine the dependence of the calculated trapping free energy on the dielectric function of the object. For a sphere in free solution carrying a uniform surface charge density, the surface may be considered to be at uniform potential so that the electric field inside the sphere is zero everywhere satisfying Laplace's equation. The potential distribution outside the sphere would thus be insensitive to changes of the dielectric medium inside and the system free energy would show no dependence on the dielectric function of the object. Constant surface charge conditions, with no stipulations on the potential of the sphere surface other than continuity, can however lead to non-zero electric fields inside the sphere. This implies that changes in the dielectric constant of the sphere interior could influence charge density distributions in the exterior, and therefore alter the free energy of the system. In particular, the presence of extraneous spatially inhomogeneous electric fields due to the proximity of charged entities, e.g., walls in this case, at distances comparable to the Debye length, could be expected to quantitatively alter the free energy of the trap. An investigation of the trap free energy as a function of dielectric constant of the sphere demonstrates that while there is some influence of particle dielectric constant on the free energy of the trap, the effect may be neglected for all practical purposes (Fig. 4). Indeed, the interior of the sphere is generally omitted from consideration altogether, i.e., ε_p is set to 0, in interaction energy calculations.[28] Neglecting the interior of the sphere in these calculations is further warranted from an experimental perspective: in many cases, net surface charge on high dielectric or conductive metal particles in solution is conferred by a thin low dielectric layer such as a self-assembled monolayer of organic molecules bearing a charged end group.[15] Calculations show that the presence of a thin low-dielectric region suffices to entirely mask the effect of the conductive interior. The open symbol in Fig. 4 denotes the well depth calculated for a 76 nm diameter conductive particle surrounded by a 2 nm thick dielectric shell, which is only ~1% smaller than for an 80 nm sphere with $\varepsilon_p = 0$. The negligible effect of the dielectric properties of the trapped

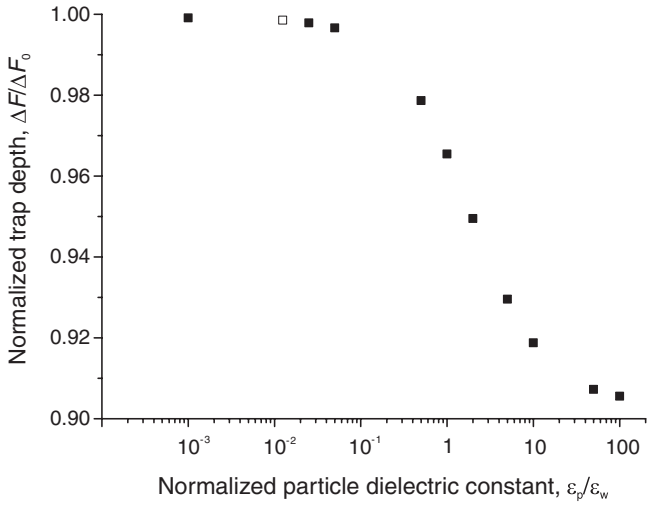

FIG. 4. Dependence of the trap depth on particle dielectric constant. Well depths calculated for a particle of variable dielectric constant ε_p and radius $a = 40$ nm, in an aqueous electrolyte of concentration $c_0 = 0.03$ mM and dielectric constant $\varepsilon_w = 80$, for particle and wall surface charge densities $\sigma_p = -3 \times 10^{-3}$ e/nm^2 and $\sigma_w = -10^{-2}$ e/nm^2. The open symbol denotes a metallic particle of radius $a = 38$ nm surrounded by a 2 nm thick dielectric region where the interior and exterior values of the normalized dielectric constant are $\varepsilon_p/\varepsilon_w = 100$ and 0.025, respectively. All free energies are normalized by $\Delta F_0 = 5.3\ k_BT$, the well depth for a particle with $\varepsilon_p = 0$. Here, "well depth" denotes the difference in system free energy when the particle is located at $r = 75$ nm with reference to the value at $r = 0$, the bottom of the well.

object not only aids in simplifying the numerical computation but has important implications from a practical standpoint: it frees this technique of the strong dependence on object mass and dielectric contrast that inherently limits trapping methodologies that rely on the bulk polarizability of matter. This is exemplified in the recently demonstrated stable electrostatic trapping of charged aqueous lipid vesicles in water,[7] which may be viewed as infinitesimally thin closed charged shells, with the same dielectric medium both on the inside and outside.

C. Trapping an uncharged object

In order to investigate the role of object charge on the spatial free energy modulation, we turned off the surface charge of the object ($\sigma_p = 0$) and repeated the calculation with slit walls of constant surface charge. Well depths for different particle sizes and system ionic strengths were determined by taking the difference of system free energy for situations where the particle is at loci representing the bottom of the well and completely outside the indentation, at $r = 200$ nm (Fig. 5(b)). We note substantial free energy differences $> 10\ k_BT$ for larger objects implying that even an object carrying no electrical charge may be spatially trapped. For example, in the case of intermediate salt concentration in Fig. 5, a 140 nm diameter particle carrying no charge may be stably trapped and levitated for over 2 h. Although this result may initially seem counterintuitive, it is founded in the fact that the physics of the trap largely rests on the configurational entropy of the counterions in the system, which come both from the object as well as the slit walls. In the absence of surface charge on the particle, the available wall counterions behave as an "ideal

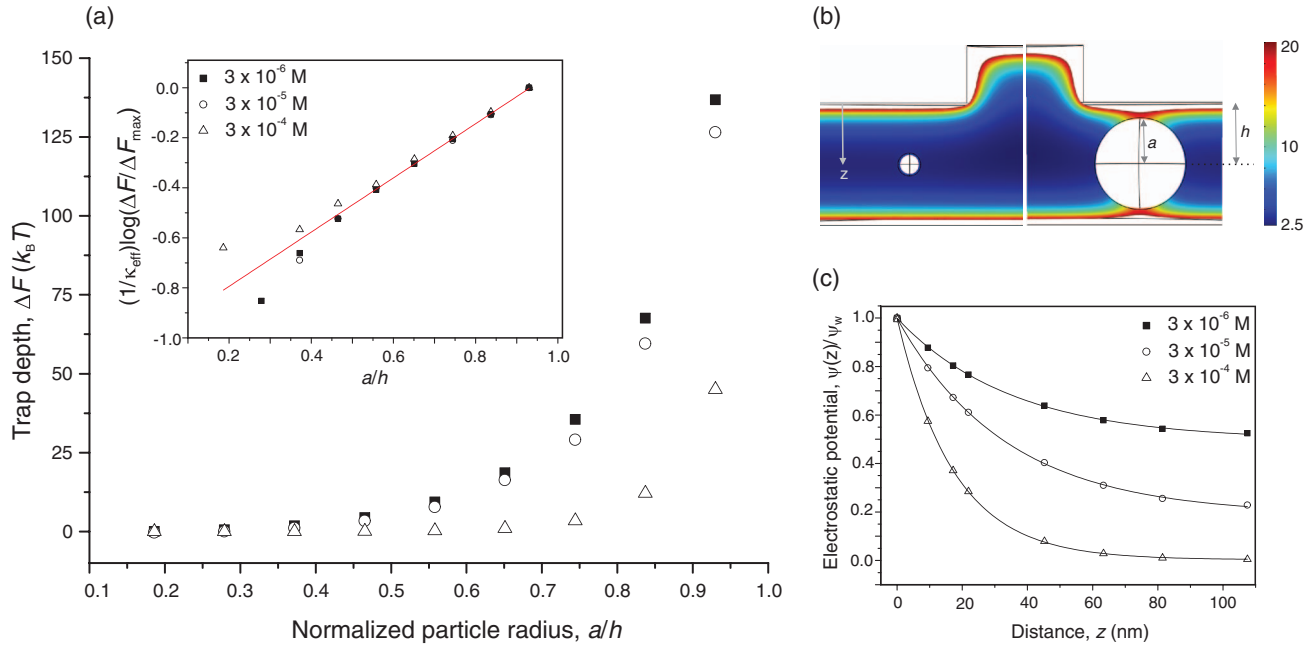

FIG. 5. Trapping an uncharged particle. (a) Well depth as a function of particle radius a, based on free energy differences with the particle positioned at axial minima at $r = 0$, and outside the well in the slit region at $r = 200$ nm, for three salt concentrations $c_0 = 0.003$, 0.03 and 0.3 mM, with $h = 107.5$ nm and wall surface charge density $\sigma_w = -10^{-2}$ e/nm^2.The inset displays the same data rescaled by the effective Debye length, κ_{eff}^{-1} (obtained as described in (c)) after subtraction of an offset given by the trap depth, ΔF_{max} at $a/h = 0.93$ in each case. A collective fit to the data (red line) yields a straight line of slope $= 0.99 \pm 0.01$, revealing an exponential dependence of well depth on particle size for $a/h > 0.5$. (b) Cross-section of spatial counterion density distributions in the yz plane depicted for particles of radius $a = 20$ nm (left) and $a = 80$ nm (right), located outside the well at $r = 200$ nm, with $c_0 = 0.003$ mM. The scale bar is in units of c_0. (c) Exponential fits to the axial electrostatic potential decay from a slit wall, far away from the particle, along the white arrow depicted in (b) yield effective Debye lengths, $\kappa_{eff}^{-1} = 35.1$, 33.5 and 17.3 nm and wall surface potentials $\psi_w = -140$, -83 and -36 mV for salt concentrations $c_0 = 0.003$, 0.03 and 0.3 mM, respectively.

gas" whose distribution is perturbed by the intruding object. In other words, counterion entropy repels the sphere out of the parallel plate zone, into the trap.

Continuing our analysis on the dependence of well depth on the size of an uncharged particle, we find that for large particles that occlude a substantial fraction of the slit depth, $a/h > 0.5$ the plot reveals an exponential dependence of trap depth on particle size, with different decay parameters for three different ionic strengths tested (Fig. 5(a)). Figure 5(c) plots the decay of electrostatic potential from the slit surface far away from the particle from which we extract a decay constant that we refer to as the effective Debye length, κ_{eff}^{-1}. Note that in the regime $\kappa^{-1} \sim h$, owing to the proximity of the walls the effective decay constant of the potential near a surface can be smaller than κ^{-1}, the free surface value. Accounting for the effective Debye length and removing an offset at each of the three ionic strengths, collapses the data on a single line suggesting a generalized exponential dependence of trap depth on particle size, $\Delta F \sim \exp(a\kappa_{eff})$ (inset of Fig. 5(a)). This is reminiscent of the exponentially decaying interaction energy $U \sim \exp(-\kappa x)$ between two parallel plates with an intersurface separation $x = h - a$, which may be expected to apply for the sphere-wall interaction in the regime $x < a$ discussed here. Further analyzing the self-energy and entropic contributions reveals that for an uncharged object, the self-energy of the system actually works against the entropy. We recapitulate that for the charged object – both at constant surface charge and potential – though the self-energy term is small, it nonetheless contributes toward rather than detracting from the total trap depth. The case of the uncharged object thus raises prospects for electrostatic trapping of a nanoscale entity solely by virtue of counterion entropy.

III. DISCUSSION

Recent MD simulations have confirmed the presence of a dramatically lower dielectric constant within 0.5 nm from a charged surface in contact with water.[29] This low dielectric region is thought to function as the phenomenological Stern layer and has successfully explained a number of experimental conundrums in the electrokinetic properties of charged interfaces. Although our current analysis invokes a net surface charge that includes the contribution of the Stern layer, the geometry may be easily modified to include the low dielectric interfacial region and bare surface charge density of the material. Furthermore, although mean field considerations have been ubiquitously and successfully applied to explain electrostatic interactions in bulk soft matter, there exist experimental observations, e.g., in the interactions of like-charged entities in monovalent salt, both in free solution and in confinement, that are at odds even qualitatively with the existing theoretical framework.[6,30–32] A detailed understanding of the scope of mean field theory is therefore particularly relevant for nanoscale systems where contributions from processes, e.g., Manning condensation or fluctuation forces may need to be included in order to explain dramatic deviations of particular experimental observations from theory.[33,34] Our calculations provide a platform for rigorous comparisons of observations with theory and thus not only lay the framework for new measurement tools,[25] but will also contribute to the development of quantitative approaches to the control and manipulation of mesoscopic matter in fluids.

[1] J. O. Tegenfeldt, C. Prinz, H. Cao, S. Chou, W. W. Reisner, R. Riehn, Y. M. Wang, E. C. Cox, J. C. Sturm, P. Silberzan, and R. H. Austin, Proc. Natl. Acad. Sci. U.S.A. **101**, 10979 (2004).
[2] W. Reisner, N. B. Larsen, H. Flyvbjerg, J. O. Tegenfeldt, and A. Kristensen, Proc. Natl. Acad. Sci. U.S.A. **106**, 79 (2009).
[3] J. Han, S. W. Turner, and H. G. Craighead, Phys. Rev. Lett. **83**, 1688 (1999).
[4] J. Fu, R. B. Schoch, A. L. Stevens, S. R. Tannenbaum, and J. Han, Nat. Nanotechnol. **2**, 121 (2007).
[5] J. D. Cross, E. A. Strychalski, and H. G. Craighead, J. Appl. Phys. **102**, 024701 (2007).
[6] M. Krishnan, I. Monch, and P. Schwille, Nano Lett. **7**, 1270 (2007).
[7] M. Krishnan, N. Mojarad, P. Kukura, and V. Sandoghdar, Nature (London) **467**, 692 (2010).
[8] M. Celebrano, C. Rosman, C. Sonnichsen, and M. Krishnan, Nano Lett. **12**, 5791 (2012).
[9] K. Xiao and D. G. Grier, Phys. Rev. Lett. **104**, 028302 (2010).
[10] M. P. MacDonald, G. C. Spalding, and K. Dholakia, Nature (London) **426**, 421 (2003).
[11] R. Dangla, S. Lee, and C. N. Baroud, Phys. Rev. Lett. **107**, 124501 (2011).
[12] P. Bahukudumbi and M. A. Bevan, J. Chem. Phys. **126**, 244702 (2007).
[13] F. Soyka, O. Zvyagolskaya, C. Hertlein, L. Helden, and C. Bechinger, Phys. Rev. Lett. **101**, 208301 (2008).
[14] M. B. Hochrein, J. A. Leierseder, L. Golubovic, and J. O. Radler, Phys. Rev. Lett. **96**, 038103 (2006).
[15] D. A. Walker, B. Kowalczyk, M. O. de la Cruz, and B. A. Grzybowski, Nanoscale **3**, 1316 (2011).
[16] D. A. Walker, C. E. Wilmer, B. Kowalczyk, K. J. M. Bishop, and B. A. Grzybowski, Nano Lett. **10**, 2275 (2010).
[17] R. Karnik, C. Duan, K. Castelino, H. Daiguji, and A. Majumdar, Nano Lett. **7**, 547 (2007).
[18] Z. Jiang and D. Stein, Phys. Rev. E **83**, 031203 (2011).
[19] H. A. Kramers, Physica **7**, 284 (1940).
[20] J. T. G. Overbeek, Colloids Surf. **51**, 61 (1990).
[21] D. Stigter, Biophys. J. **69**, 380 (1995).
[22] M. Ospeck and S. Fraden, J. Chem. Phys. **109**, 9166 (1998).
[23] M. Dubois, T. Zemb, L. Belloni, A. Delville, P. Levitz, and R. Setton, J. Chem. Phys. **96**, 2278 (1992).
[24] F. Tessier and G. W. Slater, Electrophoresis **27**, 686 (2006).
[25] N. Mojarad and M. Krishnan, Nat. Nanotechnol. **7**, 448 (2012).
[26] J. Stankovich and S. L. Carnie, Langmuir **12**, 1453 (1996).
[27] S. H. Behrens and M. Borkovec, Phys. Rev. E **60**, 7040 (1999).
[28] S. L. Carnie, D. Y. C. Chan, and J. Stankovich, J. Colloid Interface Sci. **165**, 116 (1994).
[29] D. J. Bonthuis, S. Gekle, and R. R. Netz, Phys. Rev. Lett. **107**, 166102 (2011).
[30] M. Krishnan, Z. Petrasek, I. Moench, and P. Schwille, Small **4**, 1900 (2008).
[31] M. Polin, D. G. Grier, and Y. Han, Phys. Rev. E **76**, 041406 (2007).
[32] P.-K. Lin, K.-h. Lin, C.-C. Fu, K. C. Lee, P.-K. Wei, W.-W. Pai, P.-H. Tsao, Y. L. Chen, and W. S. Fann, Macromolecules **42**, 1770 (2009).
[33] M. Kardar and R. Golestanian, Rev. Mod. Phys. **71**, 1233 (1999).
[34] G. S. Manning, Eur. Phys. J. E **34**, 132 (2011).